RNA-Sequencing Gene Expression Profiling of Orbital Adipose-Derived Stem Cell Population Implicate *HOX* Genes and WNT Signaling Dysregulation in the Pathogenesis of Thyroid-Associated Orbitopathy

Wensi Tao,[1] Juan A. Ayala-Haedo,[1] Matthew G. Field,[2] Daniel Pelaez,[1,3] and Sara T. Wester[1]

[1]Dr. Nasser Al-Rashid Orbital Vision Research Center, Bascom Palmer Eye Institute, Department of Ophthalmology, University of Miami Miller School of Medicine, Miami, Florida, United States
[2]The Sheila and David Fuente Graduate Program in Cancer Biology, Sylvester Comprehensive Cancer Center, University of Miami Miller School of Medicine, Miami, Florida, United States
[3]Department of Biomedical Engineering, University of Miami Miller School of Medicine, Miami, Florida, United States

Correspondence: Sara T. Wester, Department of Ophthalmology, Bascom Palmer Eye Institute, Room 804, McKnight Vision Research Center, 1638 NW 10th Avenue, University of Miami School of Medicine, Miami, FL 33136, USA;
swester2@med.miami.edu.

Submitted: May 18, 2017
Accepted: October 17, 2017

Citation: Tao W, Ayala-Haedo JA, Field MG, Pelaez D, Wester ST. RNA-sequencing gene expression profiling of orbital adipose-derived stem cell population implicate *HOX* genes and WNT signaling dysregulation in the pathogenesis of thyroid-associated orbitopathy. *Invest Ophthalmol Vis Sci.* 2017;58:6146–6158. DOI:10.1167/iovs.17-22237

Purpose. The purpose of this study was to characterize the intrinsic cellular properties of orbital adipose-derived stem cells (OASC) from patients with thyroid-associated orbitopathy (TAO) and healthy controls.

Methods. Orbital adipose tissue was collected from a total of nine patients: four controls and five patients with TAO. Isolated OASC were characterized with mesenchymal stem cell–specific markers. Orbital adipose-derived stem cells were differentiated into three lineages: chondrocytes, osteocytes, and adipocytes. Reverse transcription PCR of genes involved in the adipogenesis, chondrogenesis, and osteogenesis pathways were selected to assay the differentiation capacities. RNA sequencing analysis (RNA-seq) was performed and results were compared to assess for differences in gene expression between TAO and controls. Selected top-ranked results were confirmed by RT-PCR.

Results. Orbital adipose-derived stem cells isolated from orbital fat expressed high levels of mesenchymal stem cell markers, but low levels of the pluripotent stem cell markers. Orbital adipose-derived stem cells isolated from TAO patients exhibited an increase in adipogenesis, and a decrease in chondrogenesis and osteogenesis. RNA-seq disclosed 54 differentially expressed genes. In TAO OASC, expression of early neural crest progenitor marker (WNT signaling, *ZIC* genes and *MSX2*) was lost. Meanwhile, ectopic expression of *HOXB2* and *HOXB3* was found in the OASC from TAO.

Conclusion. Our results suggest that there are intrinsic genetic and cellular differences in the OASC populations derived from TAO patients. The upregulation in adipogenesis in OASC of TAO may be is consistent with the clinical phenotype. Downregulation of early neural crest markers and ectopic expression of *HOXB2* and *HOXB3* in TAO OASC demonstrate dysregulation of developmental and tissue patterning pathways.

Keywords: orbital adipose-derived stem cell, thyroid associated orbitopathy, RNA-seq

Thyroid-associated orbitopathy (TAO) is an autoimmune process associated with systemic thyroid disease,[1,2] most commonly Graves' disease (GD) and Hashimoto's thyroiditis, but also hypothyroidism, and even euthyroidism in some cases.[3,4] Expansion of the orbital tissue volume (extraocular muscles and adipose tissue) surrounding the eye may lead to exophthalmos, exposure keratopathy, and vision-threatening compressive optic neuropathy.[1,2,5]

The pathogenesis of TAO is initiated by an autoimmune cascade in which autoantibodies against thyroid-stimulating hormone receptor (TSHR) and insulin-like growth factor 1 receptor (IGF-1R) cross-react with orbital fibroblasts.[6] Activated orbital fibroblasts release chemokines, including IL-6, IL-4, IL-16, IL-1B, and monocyte chemotactic factor-1 (MCP-1), which further recruit T lymphocytes to the orbit.[7] Immunohistochemical studies have demonstrated the presence of infiltrating lymphocytes (predominantly T lymphocytes) and hyaluronan deposition in muscle and adipose tissue of patients with TAO.[8–10] Interleukin-6 has also been shown to elicit an increase in TSHR expression on orbital fibroblasts[11] as well as to program maturation and antibody production in plasma cells.[12] Meanwhile, IL-4 can induce the differentiation of naïve helper T cells into TH2 cells, mediating the immune response.[13] Monocyte chemotactic factor-1 is a potent chemoattractant that can promote the infiltration of mononuclear cells into the orbital fat pad in patients with TAO.[14] As a result, infiltrating lymphocytes can activate the orbital fibroblasts to upregulate secretion of other proinflammatory cytokines, modulate gene expression, and lead to increased cell proliferation, adipogenesis, and production of glycosaminoglycans.[15,16] Although the inflammatory response is well outlined, the pathophysiology of TAO has not been complete-

ly elucidated and the variability in disease course and presentation still remains elusive.[17,18]

The disease risk, course, and severity of TAO can be influenced by numerous genetic, epigenetic, and environmental factors.[1,19,20] Several genetic risk factors for TAO have been identified, including polymorphisms in human leukocyte antigen-DR3 (HLA-DR3),[21] cytotoxic T lymphocyte antigen (CTLA-4),[22] receptors for the interleukin family of cytokines,[23,24] and toll-like receptors.[25] Many genetic variations that have been identified in TAO are in the immunomodulatory genes, which are also associated with GD.[19] The subsets of individual genes that are specifically responsible for the local autoimmune process of TAO remain elusive.[1,26] Other than genetic factors, epigenetic factors have also been implicated in both GD and TAO. For example, more skewing of X chromosome inactivation was found in patients with autoimmune thyroid disease than in control patients.[27] Because X chromosome inactivation only happens in females (2 X chromosomes), this mechanism may partially explain the fact that there is a higher risk of GD and TAO in females than males.[27,28] Environmental factors also play important roles in both GD and TAO.[29] Smoking is a well-documented risk factor for TAO with a relative risk of 7.7 for TAO but only 1.9 for GD,[30] and it has been shown that smokers have increased soluble intercellular adhesion molecule-1 (sICAM-1) and decreased soluble vascular adhesion molecule-1 (sVCAM-1) levels.[31] There is a significant increase in the odds ratios of risk for severe TAO in patients who smoke.[30,32–34] In addition, infectious agents, such as *Yersinia enterocolitica*, can express proteins similar to the leucine-rich domain of the TSHR of the host.[35] It has been shown that B cells exposed to the bacterial antigen can also cross-react with similar domains on endogenous receptors (such as TSHR), which may lead to the development of autoimmune disease, such as GD and TAO.[36] Thus, GD and TAO are associated with many different genetic, epigenetic, and environmental factors.

To better understand which factors may be implicated in disease onset and severity, several gene expression profiling studies using microarray have been performed for TAO.[17,37,38] Many signaling pathways, such as IGF-1 and WNT signaling, have been associated with the development of TAO.[37] Interestingly, previous studies have only focused on the whole orbital adipose tissue rather than isolating the stem cell population in these tissues.[17,37,38] White adipose tissue is composed of adipocytes, fibroblasts, macrophages, adipose stem cells, neuronal cells, and endothelial cells from blood vessels. Gene expression studies of whole adipose tissue in autoimmune diseases may not filter out the differential gene expression profiles arising from the mesenchymal stem cell (MSC) fraction because of the overwhelming inflammatory response in the tissue. In fact, growing evidence indicates that local and systemic stem cells play important roles in the pathogenesis of numerous autoimmune diseases.[16,39–41] Genetic profiling of MSCs derived from patients with systemic lupus erythematosus has shown differential expression of genes involved in actin skeleton, focal adhesion, tight junction, and TGF-b pathway compared with healthy controls.[40] In patients with psoriasis, dermal mesenchymal stem cells (DMSCs) showed an upregulation of genes involved in cell proliferation, downregulation of genes related to development, and a differential expression of genes involved in angiogenesis.[41] In addition, a comparison between orbital fibroblasts and OASCs from patients with TAO suggests that the OASCs may represent a unique subpopulation of cells within the fibroblasts that have greater multipotency and a potentially immunomodulatory role.[42] Despite research on alterations in the local stem cell population in many other autoimmune diseases, we are not aware of any previous genetic profiling studies that have been performed on the OASC from TAO patients.

Recently, our group has isolated and characterized mesenchymal progenitor cells from human orbital adipose tissue.[43] Orbital adipose-derived stem cells from orbital adipose tissue can differentiate into several cell lineages, including vascular endothelial cells, chondrocytes, osteocytes, and adipocytes.[43] Therefore, we hypothesize that there are intrinsic modifications that take place at the cellular and genetic levels in the OASC populations derived from TAO patients and that the analysis of the differences in these OASC from TAO patients and controls might elucidate additional mechanisms that could be involved in the pathogenesis of TAO.

Materials and Methods

Human Adipose Tissue Collection

Samples were collected from orbital fat from control patients undergoing eyelid surgery and TAO patients undergoing orbital decompression. All patients were consented; the study was approved by the University of Miami institutional review board (protocol 20110692) and followed the tenets of the Declaration of Helsinki. Samples were adequately preserved on ice and transported within 4 hours to the laboratory and processed upon receipt.

We recruited a total of nine patients, five cases (2 patients undergoing surgery for compressive optic neuropathy and 3 for orbital rehabilitation) and four controls without history of TAO (Table 1). A chart review was performed to assess relevant patient information, including clinical activity score (CAS), smoking history, previous treatment received for orbital disease, medical co-morbidities, treatment of thyroid disease, thyroid stimulating immunoglobulin (TSI) and race.

Cell Isolation

The cell isolation was performed as we have previously described.[43] Briefly, after washing three times with PBS containing 50-μg/mL gentamicin and 1.25-μg/mL amphotericin B, fat tissues are cut into pieces of less than 5 mm in size. The same weight of tissues 0.5% (wt/vol) is subjected to digestion with 1 mg/mL of Col I (Worthington Biochemical Corp, Lakewood, NJ, USA) in a modified embryonic stem cell medium (MESCM)18 (Invitrogen, Carlsbad, CA, USA) or Dulbecco's modified Eagle's medium (DMEM; Invitrogen) containing 10% fetal bovine serum (FBS) for 3 hours on a shaker with intermittent manual shaking every 20 minutes and vigorous manual shaking for 10 seconds at the end of 3 hours before centrifugation at 300*g* for 5 minutes to collect cell pellets. Cut tissues are also digested with 1 mg/mL of Col A (Roche, Risch-Rotkreuz, Switzerland) in DMEM for 4 hours at 37°C. Digested tissues are pipetted up and down 10 times before centrifugation at 300*g* for 5 minutes to remove floating adipocytes. The pellets are resuspended in MESCM and filtered through a 70-μm nylon strainer (BD Bioscience, Franklin Lakes, NJ, USA) to yield cells in the flow through as stromal vascular fraction (SVF). Cells in SVF are treated with red cell blood cells lysis buffer to remove red blood cells and with 0.25% trypsin-EDTA to yield a single cell suspension at 37°C for 5 minutes.

Trilineage Differentiation

For assays of adipogenesis or osteogenesis, expanded single cells during passages three to five were seeded at the density of 2.5×104 cells/cm^2 in 24-well plates in DMEM with 10% FBS. At 90% confluence, the medium was switched to the adipogenesis differentiation medium or the osteogenesis

Table 1. Demographic Information on the Patients Included in the Study.

Patient No.	Study No.	Age	Status	Compressive Optic Neuropathy	CAS, 7 Point Scale	Smoker	Previous Treatment	Medical Co-Morbidities	Treatment of Thyroid Disease	Thyroid Stimulating Immuno-globulin	Race
1	OASC1	74	TAO	Present	4	No	Oral and IV steroids	DM, thyroid cancer	RAI, thyroidectomy	N/A	Non-Hispanic
2	OASC2	55	TAO	Present	4	Previous	Oral steroids	None	RAI, thyroidectomy	N/A	Non-Hispanic
3	OASC3	77	Control	N/A	N/A	No	N/A	HTN, arrhythmia	N/A	N/A	Hispanic
4	OASC11	67	Control	N/A	N/A	Previous	N/A	DM, HTN, VZV	N/A	N/A	Non-Hispanic
5	OASC5	82	Control	N/A	N/A	Previous	N/A	Morbid obesity, sleep apnea, reN/Al cyst, HTN, hyperlipidemia, GERD, COPD, CHF, cataract, hypothyroidism, arhthritis	N/A	N/A	Hispanic
6	OASC7	55	TAO	Not Present	3	Previous	IV steroids, XRT	TAO, hyperthyroidism, hypothyroidism, cataract, osteoporosis	RAI, thyroidectomy	488	Non-Hispanic
7	OASC8	66	TAO	Not Present	2	Previous	None	TAO, obesity, HTN, allergies, asthma, arthritis	Thyroidectomy ×2	509	Hispanic
8	OASC9	20	TAO	Not Present	1	No	None	TAO, asthma, anxiety, idiopathic intracranial hypertension, encephalitis, arthritis, myopia	Thyroidectomy, methimazole	472	Hispanic
9	OASC10	75	Control	N/A	N/A	No	N/A	HTN, hyperlipidemia, DM, arthritis, cancer, mitral regurgitation	N/A	N/A	Non-Hispanic

CAS, clinical activity score; DM, diabetes mellitus; HTN, hypertension; RAI, radioactive iodine; VZV, Varicella-Zoster virus; XRT, radiation therapy; GERD, gastroesophageal reflux disease; COPD, chronic obstructive pulmonary disease; CHF, congestive heart failure.

differentiation medium, respectively (Invitrogen) and changed every 3 days. After 21 days of culturing, cells were fixed with 4% formaldehyde and stained with oil red O for adipocytes by adipogenesis Assay Kit (Cayman Chemical Company, Ann Arbor, MI, USA) or with 2% Alizarin Red for osteocytes following the manufacturer's protocol. Cells with oil droplet stained by Oil Red were quantified by measuring at OD at 492 nm in triplicate cultures. Mineralized cells with positive Alizarin Red staining (Alfa Aesar, Tewksbury, MA, USA) were quantified by measuring OD at 405 nm in triplicate cultures.

For the chondrogenesis assay, pellets were prepared by spinning down 1×105 cells and incubating in a 15-mL conical tube in chondrogenesis differentiation medium (Invitrogen) with the medium changed every 3 days. After 28 days of culturing, cells were fixed with 4% formaldehyde, and stained with Alcian Blue (Merck, Darmstadt, Germany).

RNA Sequencing

RNA was extracted from passages three to five OASC cells expanded from stromal vascular fraction (SVF) with a combination of TriZol and the RNeasy Mini RNA isolation kit (QIAGEN, Valencia, CA, USA). RNA-seq libraries were prepared using the TruSeq Stranded Total RNA prep kit with Ribo-Zero Gold to remove cytoplasmic and mitochondrial rRNA according to the manufacturer's recommendation (Illumina, San Diego, CA, USA). The stem cell RNA-seq libraries were run on an Illumina NextSeq 500 sequencing instrument according to the protocols described by the manufacturer (Illumina). Reads were aligned using STAR, data quality was assessed using FastQC and RSeQC, and differential gene expression was determined using both EdgeR and DESeq2. Genes that were differentially expressed according to both EdgeR and DESeq2 were used for downstream analyses. Those differentially expressed genes with a P less than 0.005 a fold change greater than 1.5 were selected for further evaluation (Table 2).

Quantitative Real-Time PCR

Total RNA was extracted from passages three to five OASC cells expanded from SVF with a combination of TriZol and the RNeasy Mini RNA isolation kit (QIAGEN) and reverse-transcribed to complementary (c)DNAs by high-capacity cDNA transcription kit (Applied Biosystems, Foster City, CA, USA). Quantitative PCR (qPCR) was performed in triplicate. The qPCR amplification of different genes was done in a 20-µL solution containing cDNA, primers and sybr green master Mix (Applied Biosystems). The primers used for RT-PCR analysis were listed (Table 3). All quantitative real-time PCR was performed using the 7300 Real-time RT-PCR system (Applied Biosystems) according to the manufacturer's description using the following thermocycler parameters: 10 minutes of initial activation at 95°C, 40 cycles of 15-seconds denaturation at 95°C, and 1-minute annealing and extension at 60°C. The relative gene expression data was analyzed by the comparative CT method (ΔΔCT). The results were normalized to an internal control.

Phenotypic Characterization

Immediately after isolation, cells from SVF were dried to adhere on the slides and fixed with 100% cold methanol at 20°C. Alternatively, cells freshly isolated or undergoing serial passages were treated with trypsin-EDTA at 37°C for 10 minutes and centrifugation at 55g for 8 minutes at the density of 2 to 4.0×104 cells/chamber using Cytofuge (StatSpin, Inc., Norwood, MA, USA). The cytospin preparation was dried at room temperature for 5 minutes and then fixed with either

Table 2. Upregulated and Downregulated Genes in OASC Derived From TAO Patient's Orbital Fat Tissue Compared With Controls, as Analyzed Using RNA-Seq

Gene Symbol	Gene Description	Log2 Fold Change	Gene ID	*P* Value	FDR
ZIC4	Zic family member 4	−1.99866636	ENSG00000174963	6.43^{E-11}	4.68^{E-07}
ZIC2	Zic family member 2	−1.967523486	ENSG00000043355	1.01^{E-08}	2.99^{E-05}
ENPP1	Ectonucleotide pyrophosphatase/phosphodiesterase 1	−1.939286966	ENSG00000197594	3.72^{E-06}	0.004982403
WISP1	WNT1-inducible signaling pathway Protein 1	−1.718261338	ENSG00000104415	2.04^{E-06}	0.003334138
MTND1P23	Mitochondrially encoded NADH:ubiquinone oxidoreductase core subunit 1	−1.627328038	ENSG00000225972	9.87^{E-08}	0.000242258
WNT16	Wnt family member 16	−1.584685718	ENSG00000002745	0.000125	0.068012492
PSCA	Prostate stem cell antigen	−1.562039103	ENSG00000167653	0.000415	0.143845059
RP11-839G9.1	RP11-839G9.1	−1.510719098	ENSG00000267112	5.34^{E-05}	0.046207001
ZIC5	Zic family member 5	−1.495481869	ENSG00000139800	4.82^{E-05}	0.044351687
NACA3P	Nascent-polypeptide-associated complex alpha polypeptide pseudogene	−1.494574661	ENSG00000121089	0.00036	0.132375925
ULBP1	UL16 binding protein 1	−1.489832209	ENSG00000111981	0.000513	0.160627696
MSX2	Msh (drosophila) homeo box homolog 2 (*HOX8*)	−1.355828948	ENSG00000120149	0.000219	0.091914409
AD000091.3	Uncategorized gene, and is affiliated with the lncRNA class	−1.032374795	ENSG00000267135	9.25^{E-05}	0.056730134
RP11-10G12.1	Ribosomal protein S27 Pseudogene 13	−0.990929207	ENSG00000244538	0.000204	0.091101817
RPL23AP2	Ribosomal protein L23a pseudogene 2	−0.962700415	ENSG00000225067	0.000225	0.091914409
RP1-292B18.1	Ribosomal protein L32 pseudogene 16	−0.955193953	ENSG00000219747	1.29^{E-05}	0.012688179
RN7SL4P	RNA, 7SL, cytoplasmic 4, pseudogene	−0.911666602	ENSG00000263740	0.000161	0.076366012
AAED1	AhpC/TSA antioxidant enzyme domain containing 1	−0.721620492	ENSG00000158122	1.53^{E-07}	0.000321973
RPL4P5	Ribosomal protein L4 pseudogene 5	−0.586951905	ENSG00000230207	0.000212	0.091656977
LRRC1	Leucine-rich repeat containing 1	0.898179937	ENSG00000137269	0.00066	0.190470156
PHEX	Phosphate regulating endopeptidase homolog, X-linked	1.235226884	ENSG00000102174	0.000591	0.177516296
NDEL1	NudE neurodevelopment protein 1 like 1	1.292854172	ENSG00000166579	0.000442	0.14461686
CDC20P1	CDC20 cell division cycle 20 homolog pseudogene	1.34058504	ENSG00000231007	0.00043	0.144042401
IFI44L	Interferon-induced protein 44 like	1.343311517	ENSG00000137959	0.000738	0.194693727
AGT	Angiotensinogen	1.449016649	ENSG00000135744	6.05^{E-05}	0.046866148
F3	Coagulation factor III	1.462297193	ENSG00000117525	7.06^{E-05}	0.047250575
BST2	Bone marrow stromal cell antigen 2	1.468253178	ENSG00000130303	0.000335	0.129911717
ANK3	Ankyrin 3, node of ranvier (ankyrin G)	1.494958528	ENSG00000151150	0.000454	0.145406769
DSC3	Desmocollin 3	1.515448417	ENSG00000134762	0.000737	0.194693727
CFL1P3	Cofilin 1 pseudogene 3	1.556527183	ENSG00000228056	0.000566	0.173505519
PCDH10	Protocadherin 10	1.6031006	ENSG00000138650	5.38^{E-06}	0.006599162
ANO4	Transmembrane protein 16D	1.605824767	ENSG00000151572	5.65^{E-05}	0.046207001
RP4-597J3.1	Ribosomal protein L19 Pseudogene 3	1.639432645	ENSG00000177452	0.000154	0.076366012
RP11-388P9.2	An RNA gene	1.649482498	ENSG00000232682	0.000618	0.181964905
COL15A1	Collagen-yype XV alpha 1 chain	1.686957187	ENSG00000204291	0.000109	0.061887348
PDLIM3	PDZ And LIM domain 3	1.692324946	ENSG00000154553	0.000372	0.133610896
KAL1	Anosmin 1	1.704051374	ENSG00000011201	0.000193	0.088717352
RP11-993B23.3	An RNA gene	1.727559788	ENSG00000257042	7.81^{E-06}	0.00884094
ADCY2	Adenylate cyclase 2	1.730203161	ENSG00000078295	0.000344	0.130016512
GLDN	Gliomedin	1.730961059	ENSG00000186417	3.65^{E-06}	0.004982403
RP11-92C4.6	Antisense RNA class	1.754612068	ENSG00000270412	9.72^{E-05}	0.05725544
FAM155A	Family with sequence similarity 155 member A	1.781252892	ENSG00000204442	0.000698	0.194693727
PTGDR	Prostaglandin D2 receptor (DP)	1.787182341	ENSG00000168229	6.89^{E-05}	0.047250575
HOXB3	Homeobox B3	2.023921886	ENSG00000120093	8.34^{E-05}	0.053413413
ARHGDIB	Rho GDP dissociation inhibitor beta	2.030211894	ENSG00000111348	0.000157	0.076366012
SPON1	Spondin 1, (F-Spondin) extracellular matrix protein	2.051744968	ENSG00000262655	0.000131	0.068727393
HOXB-AS1	*HOXB* cluster antisense RNA 1 (nonprotein coding)	2.062884891	ENSG00000230148	0.000297	0.118049004
RP4-678D15.1	An RNA gene	2.115270914	ENSG00000271774	0.00042	0.143845059
RP11-21L19.1	An RNA gene	2.297884718	ENSG00000254418	6.52^{E-05}	0.047250575
KCNA4	Potassium voltage-gated channel subfamily A member 4	2.565790939	ENSG00000182255	3.50^{E-07}	0.000643565
S100B	S100 calcium-binding protein B	2.795342911	ENSG00000160307	7.98^{E-09}	2.94^{E-05}
HOXB2	Homeobox B2	3.321078224	ENSG00000173917	1.19^{E-05}	0.012552207
CTD-2012M11.3	An RNA gene	3.583507162	ENSG00000259603	9.54^{E-11}	4.68^{E-07}
IRX1	Iroquois homeobox protein 1	4.236731758	ENSG00000170549	1.97^{E-13}	2.91^{E-09}

Investigative Ophthalmology & Visual Science

Table 3. List of Primers Used for RT-PCR Analysis

Gene	Sequence (5′->3′)
WNT16	
Forward primer	TACAGCTCCCTGCAAACGAG
Reverse primer	TGCCCAACCACATCCAGTTT
HOXB2	
Forward primer	CTCCCCCTCCCAAAATCGC
Reverse primer	GGGAAGGTTTGCTCGAAAGG
ZIC4	
Forward primer	GGCCAACCACATTTGCTTCT
Reverse primer	CTCCCCTCAGTTGGGACTTG
DSC3B	
Forward primer	AGTGTGCTCTGCCAATGGAT
Reverse primer	AACCAGTGTGTCCTCTAATGG
KCNA4	
Forward primer	CGACAGGGATCTCGTCATGG
Reverse primer	GTCAGTGCCCAGTGTGATGA
18S rRNA	
Forward primer	CGGCTACCACATCCAAGGAA
Reverse primer	GCTGGAATTACCGCGGCT
C/EBPα	
Forward primer	AAGAAGTCGGTGGACAAGAACAG
Reverse primer	TGCGCACCGCGATGT
PPARγ	
Forward primer	GATACACTGTCTGCAAACATATCACAA
Reverse primer	CCACGGAGCTGATCCCAA
FABP4	
Forward primer	GCTTTGCCACCAGGAAAGTG
Reverse primer	ATGGACGCATTCCACCACCA
Osteopontin	
Forward primer	TTGCAGCCTTCTCAGCCAA
Reverse primer	GGAGGCAAAAGCAAATCACTG
CBFA 1	
Forward primer	ATGTGTGTTTGTTTCAGCAGCA
Reverse primer	TCCCTAAAGTCACTCGGTATGTGTA
Osteocalcin	
Forward primer	CGCCTGGGTCTCTTCACTAC
Reverse primer	CTCACACTCCTCGCCCTATT
collagen II	
Forward primer	CTGGTGATGATGGTGAAG
Reverse primer	CCTGGATAACCTCTGTGA
collagen x	
Forward primer	AGAATCCATCTGAGAATATGC
Reverse primer	CCTCTTACTGCTATACCTTTAC

100% cold methanol at −20°C or 4% paraformaldehyde for 15 minutes at room temperature. For immunofluorescence staining, samples were permeabilized with 0.2% Triton X-100 in PBS for 15 to 30 minutes and blocked with 0.2% BSA in PBS for 1 hour at room temperature before the addition of the primary antibody overnight at 4°C. Primary antibodies used for staining are listed (Table 4). Isotype-matched nonspecific IgG antibodies were used as controls. Image analysis was performed using confocal laser microscopy (LSM700; Carl Zeiss, Inc., Thornwood, NY, USA).

Results

Characterization of OASCs by Stem Cell Markers

The purpose of this study was to determine the molecular characteristics of OASC from TAO patients. We have previously demonstrated that OASC isolated from orbital adipose tissue express progenitor and stem cell markers.[43] In the current study, immunofluorescence staining with stem cell markers was performed to characterize the OASCs of controls and TAO. The OASC expressed low levels of pluripotent stem cell markers (KLF4, OCT4, Nanog, and Sox2) (Fig. 1A). However, high expression levels of mesenchymal stem cell markers (CD 90, Nestin, CD146, and PDGFR) were found in these OASCs, and were similar in both TAO and controls (Fig. 1B). These data suggest that OASC may be progenitor cells for mesenchymal lineage.

Table 4. List of Primary Antibodies Used for Staining

Antibody	Supplier	Source	Dilution
Oct3/4	Cell Signaling Technology (Danvers, MA, USA)	Rabbit	200
Nanog	Cell Signaling Technology	Rabbit	200
Sox2	Cell Signaling Technology	Rabbit	200
Klf4	Cell Signaling Technology	Rabbit	200
Lin28	Cell Signaling Technology	Rabbit	200
PDGFR	Abcam (Cambridge, United Kingdom)	Rabbit	200
CD90	Abcam	Rabbit	200
CD146	Abcam	Rabbit	200
Nestin	Abcam	Mouse	200
Ckit	Cell Signaling Technology	Rabbit	200

OASC Differentiation Into Mesenchymal Lineages

To further test the differentiation capacity of OASC as mesenchymal progenitor cells, OASC from TAO and controls were then differentiated into adipocyte, osteocyte, and chondrocyte lineages as described previously.[43]

OASC From TAO Patients Have a Higher Adipogenic Capacity

We next compared the adipogenic capacity of OASC from TAO and control patients. Orbital adipose-derived stem cells were differentiated into adipocyte lineage by adipogenic cocktails, consisted of insulin dexamethasone and 3-isobutyl-1-methylxanthine or vehicle control (DMSO). Adipogenic cocktails are capable of inducing adipogenesis in vitro. After 21 days of culturing, by oil red O staining, we visualized and quantified the content of neutral lipid droplets in the adipocytes. Orbital adipose-derived stem cells from TAO patients demonstrated an increase in the adipogenesis capacity, as stained with oil red O and identified by their bright red color (Fig. 2A). The stained oil red O was extracted with 100% isopropanol and quantified by the absorbance. Higher absorbance of extracted oil red O dye in the OASC from TAO patients suggested that OASC from diseased orbit had higher adipogenic differentiation capacity than controls (Fig. 2A). Quantitative RT-PCR was used to confirm the upregulation in adipogenesis with the selected genes involved in the adipogenesis process. Three adipocyte differentiation markers (PPAR-g, C/EBP-a, and FABP4) were upregulated in the OASC from TAO patients when compared with controls (Fig. 2B). These obtained data suggested that OASC from diseased orbit have a higher adipogenic capacity.

OASC From TAO Have a Lower Osteogenic Capacity

Furthermore, we compared the osteogenic capacity of OASC from TAO and control patients. Orbital adipose-derived stem cells were differentiated into osteocyte lineage by switching to osteocyte differentiation medium. After 21 days of culturing, osteogenesis was assayed by Alizarin Red S staining for

Investigative Ophthalmology & Visual Science

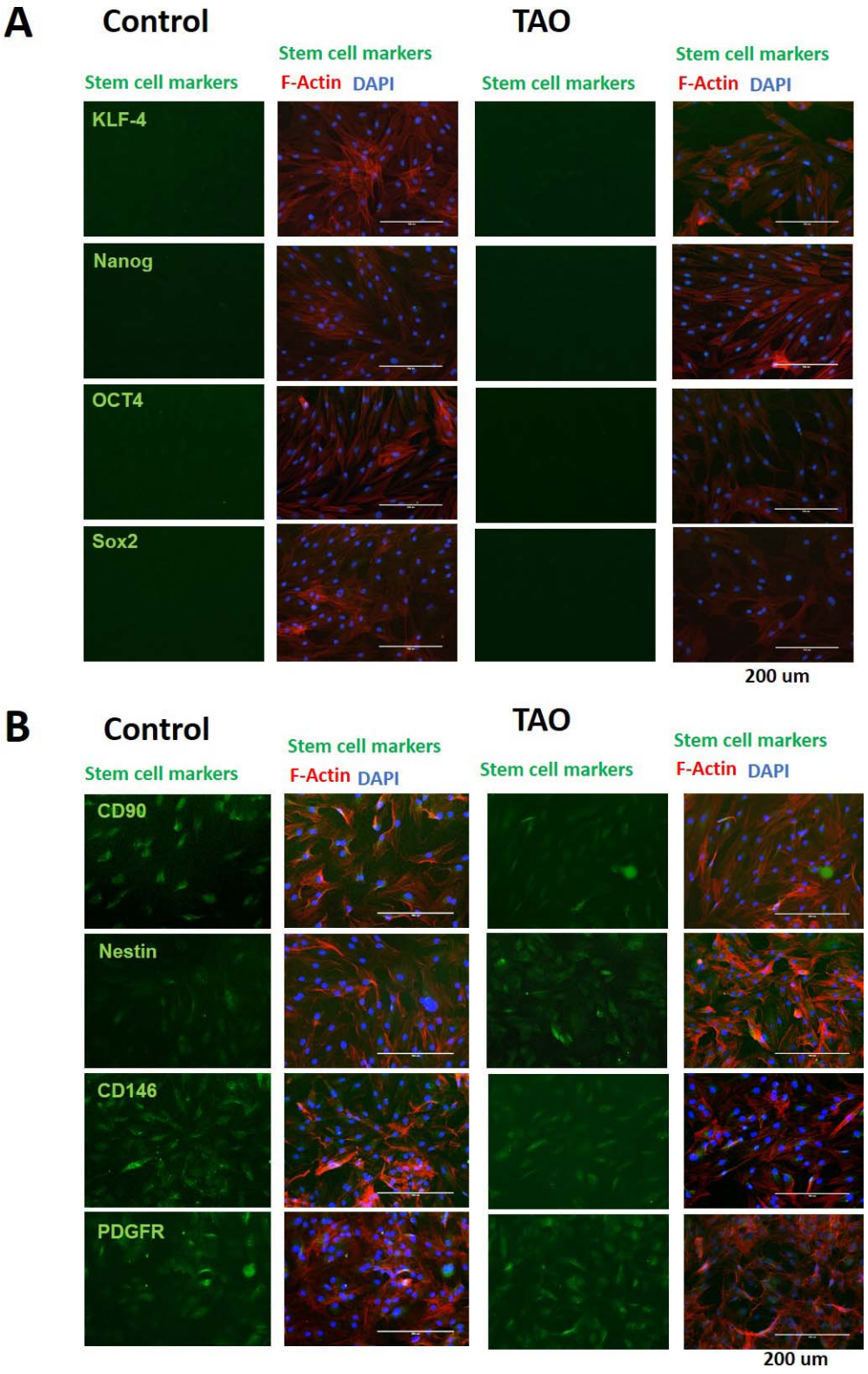

Figure 1. Immunofluorescence staining of OASC for stem cell markers from TAO and control. Orbital adipose-derived stem cells were stained with (**A**) pluripotent stem cell markers (KLF4, OCT4, Nanog, Sox2) and (**B**) mesenchyme stem cell markers (DC 90, Nestin, CD146, PDGFR) in samples from control adipose tissue. *Left column* has stem cell markers (*green*), the *right column* has the merged photographs, including stem cell markers (*green*), F-actin (marker for cytoskeleton, *red*), and 4′,6-diamidino-2-phenylindole (DAPI) (a marker for cell nuclei, *blue*).

Investigative Ophthalmology & Visual Science

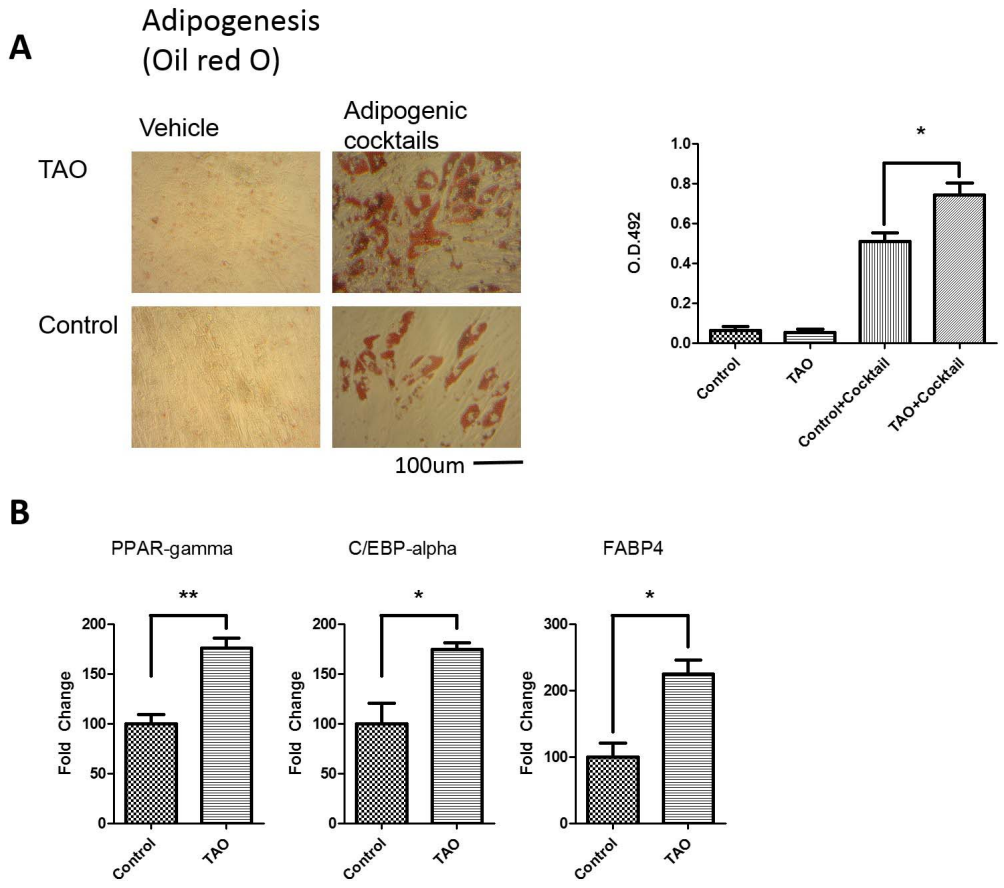

Figure 2. Adipocyte differentiation and cellular characterization. (**A**) Orbital adipose-derived stem cells cell culture samples from TAO and controls patients were differentiated into adipocyte lineage. Representative images of lipid droplet stained with Oil Red O in differentiated OASC are shown. (**B**) Quantitative RT-PCR was used to confirm upregulation in adipogenesis with the selected genes involved in the adipogenesis process. The three genes selected *PPAR-g*, *C/EBP-a*, and *FABP4* were assayed (*$P < 0.05$, **$P < 0.01$).

intracellular calcium levels. Orbital adipose-derived stem cells from TAO patients demonstrated a decrease in the osteogenic capacity, as stained with Alizarin Red S and identified by the red color (Fig. 3A). To quantify the levels of osteogenesis, Alizarin Red S was extracted and detected calorimetrically by absorbance. Orbital adipose-derived stem cells from TAO patients demonstrated a decrease in the osteogenesis capacity, as indicated by quantification of Alizarin Red S staining (Fig. 3A). Quantitative RT-PCR was used to assay osteogenesis with the selected genes *CBFA*, osteopotin, and osteocalcin. All the osteogenesis markers were downregulated in the OASC from TAO patients when compared with controls (Fig. 3B). These results indicated that OASC from TAO might have a lower osteogenic capacity.

OASC From TAO Have a Lower Chondrogenic Capacity

Then we compared the chondrogenic capacity of OASC from TAO and control patients. Similarly, OASC were differentiated into chondrocyte lineage by switching to chondrocyte differentiation medium. After 28 days of culturing, chondrogenesis was assayed by Alcian Blue staining for acidic polysaccharides. Orbital adipose-derived stem cells cell culture samples from TAO patients demonstrated a decreased staining with Alcian Blue (Fig. 4A). Quantitative RT-PCR was used to assay chondrogenesis with the selected genes Collagen X and Collagen 2. Both of the chondrogenesis markers were downregulated in the OASC from TAO patients when compared with controls (Fig. 4B). These data indicated that OASC from TAO might have a lower chondrogenic capacity.

Gene Expression Profiling of OASC From TAO Patients by RNA Sequencing Analysis

Last, we aimed to identify differentially expressed genes of OASC isolated from TAO patients' orbital fat. The patients were classified according to the presence or absence of compressive optic neuropathy at the time of surgery (3 decompressions were performed for orbital rehabilitation; Table 1). After isolation and expansion of OASC from TAO and control tissues, total messenger RNA sequencing was performed and analyzed. Differentially regulated genes with a P less than 0.005 ($n = 156$) were used for gene ontology analysis (Table 2) and were plotted in a heatmap (Fig. 5A). The top five gene ontology results were tissue development, regulation of multicellular organismal development, extracellular space, cell development, and system process (false discovery rate [FDR] < 0.001), which are all consistent with TAO adipose stem cells being actively involved in altering the tissue structure of the orbital fat pockets.

For further analysis, a more stringent filter was used ($P < 0.0005$ and fold change > 1.5) to identify the most promising genes that may be involved in promoting these alterations. Out of 54 genes that were selected with these inclusion criteria, four *HOX* family genes were upregulated (*IRX1*, *HOXB2*, *HOXB3*, *HOXB3-AS1*) and two genes in the WNT signaling pathways (*WNT16*, *WISP1*), three *ZIC* genes (*ZIC4*, *ZIC2*, *ZIC5*), and one *HOX* gene (*MSX2*) were downregulated.

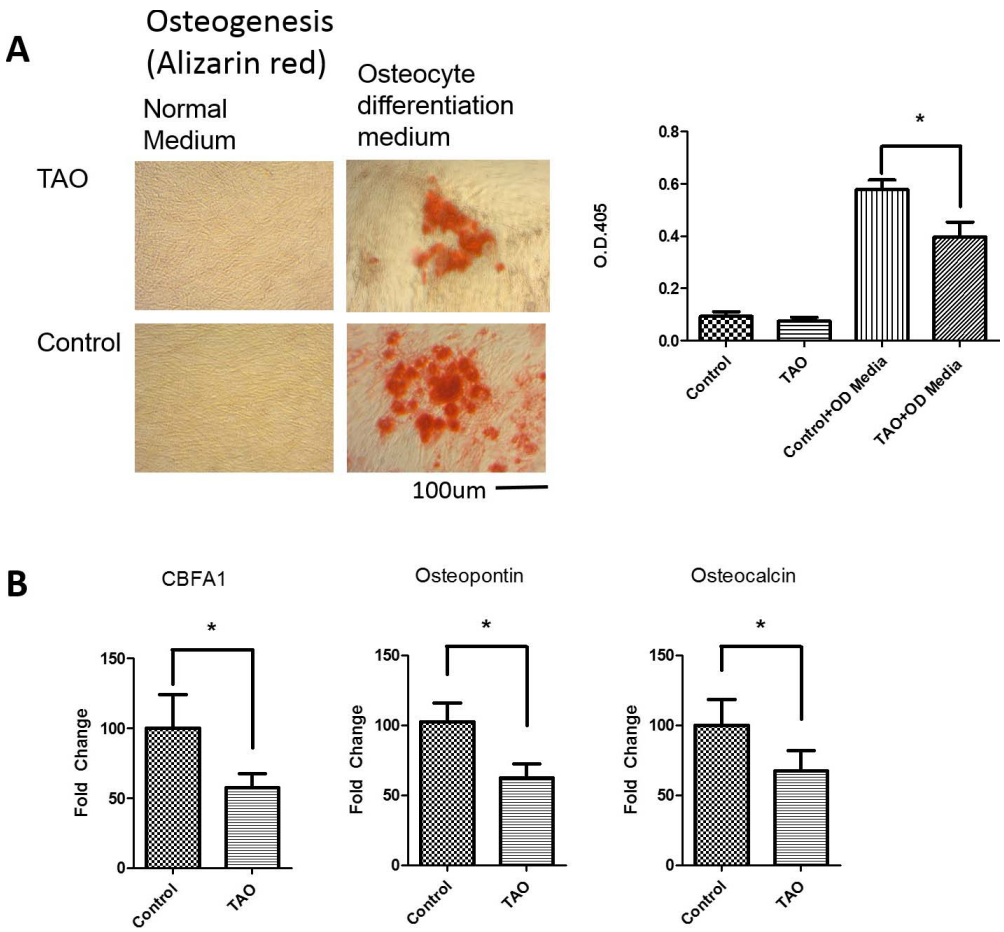

Figure 3. Osteocyte differentiation of OASC. (**A**) Alizarin Red S staining for osteogenesis in OASC cell culture sampled from TAO and controls patients. (**B**) Quantitative RT-PCR was used to confirm upregulation of osteogenesis with the selected genes *CBFA*, Osteopotin, and Osteocalcin. $^{*}P < 0.05$.

Discussion

In this study, we report the differential gene expression profiling of OASC from TAO patients and controls. While our data revealed several differentially expressed gene profiles between diseased and control patients, we found that genes related to developmental morphogenesis and lineage commitment were predominantly dysregulated in TAO. Unlike previous gene expression profiling studies that analyzed orbital fat pads and extraocular muscle,[17,38,44] the current study did

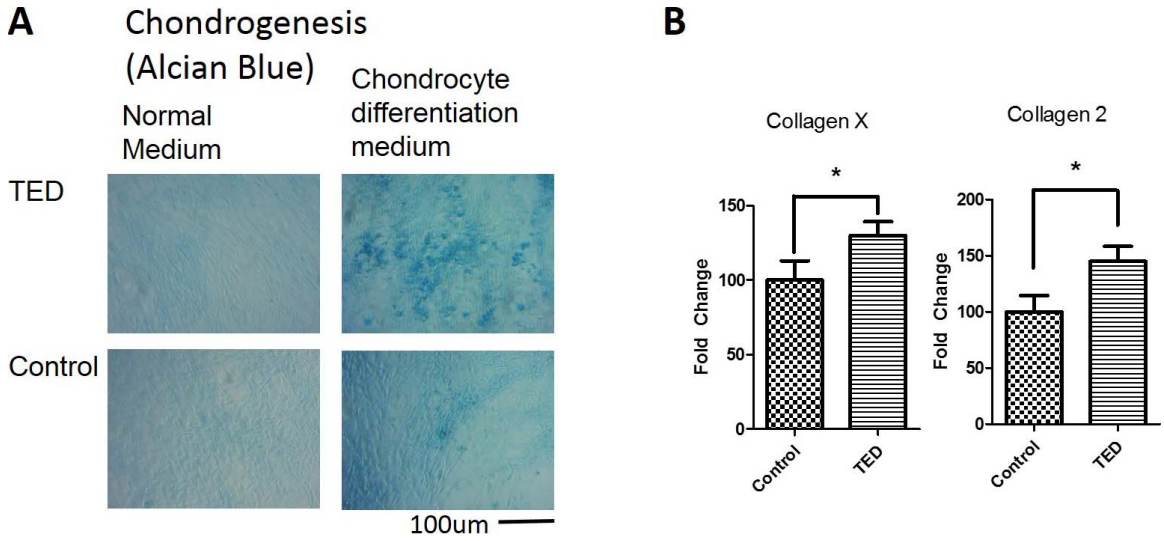

Figure 4. Chondrocyte differentiation of OASC. (**A**) Alcian Blue staining for chondrogenesis assay in OASC cell culture samples from TAO and controls patients. (**B**) Quantitative RT-PCR was used to confirm upregulation of chondrogenesis genes Collagen X and Collagen 2. $^{*}P < 0.05$.

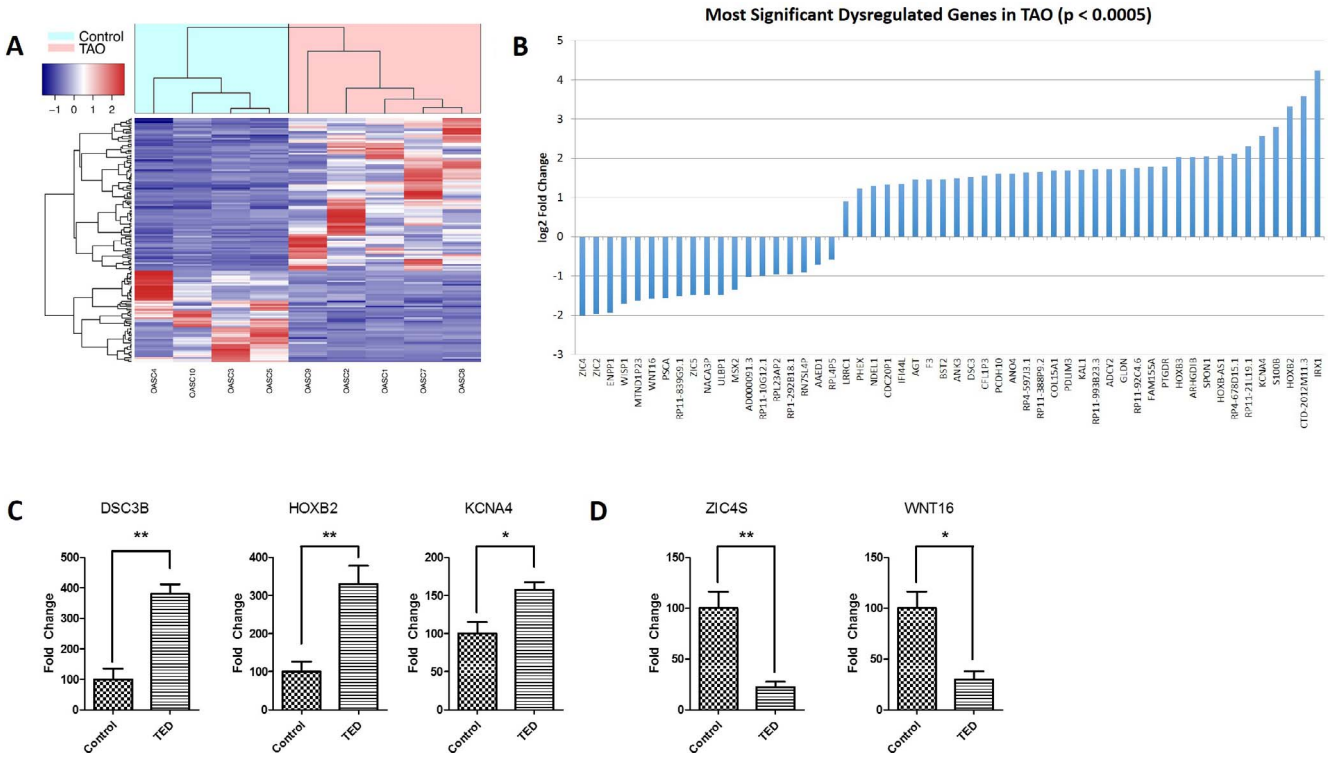

FIGURE 5. RNA-sequencing analysis of OASC from TAO patients. RNA sequence analysis was performed with the OASC from TAO patients and controls. From the genes that showed differential expression, the ones with $P < 0.005$ ($n = 156$) were plotted in a heatmap (**A**) and in a table (**B**). Reverse transcription PCR results from differentially expressed genes in RNA sequencing analysis comparing controls and TAO cases. Reverse transcription PCR results from three upregulated genes *DSC3B*, *HoxB2*, and *KCNA4* (**C**) and two downregulated genes *ZIC45* and *WNT16* (**D**) $^{*}P < 0.05$, $^{**}P < 0.01$.

not detect any significant different expression in genes related to inflammation (RNAseq dataset, Table 2). These findings suggest that our data may reveal the intrinsic cellular characteristics of the stem cell niche that are otherwise masked by the massive immunogenic response in the tissue from TAO patients. Extrinsic factors such as inflammatory cytokines are less likely to be detected by RNA-Seq because they are diluted over the passages in cell culture system. Our findings also suggested that the genetic expression differences in the stem cell populations of TAO might be related to developmental origins, such as *HOX* genes and early neural crest development. The top five gene ontology results identified from our RNA-Seq were tissue development, regulation of multicellular organismal development, extracellular space, cell development, and system process (FDR < 0.001). These are all related to the developmental origins of OASC and may affect how these cells are implicated in tissue remodeling of the orbital fat pockets in TAO.

Loss of WNT Signaling in TAO Promotes Adipogenesis

Progenitor cells for neural crest lineage are capable of differentiating into adipocytes, osteocytes, and chondrocytes.[45] Many intracellular signaling pathways tightly regulate these differentiation processes. It is well known that canonical WNT signaling regulates the neural crest progenitor cell fate.[46] Similarly, activation of WNT/Beta-catenin pathway will suppress commitment to the adipocyte lineage while promoting differentiation into osteocytes by stimulating Runx2 expression.[47,48] Previous gene expression profiling studies using whole orbital fat pads have also identified dysregulation of *WNT* in TAO patients.[37,49] The OASC compartment represents the stem/progenitor cell population of orbital fat and only account for a small portion of cells in the orbital fat pad. Our results demonstrated that *WNT* signaling was significantly suppressed in the OASC populations derived from TAO patients. Downregulation of *WNT* signaling pathways in the OASC from TAO patients can lead to the expansion of a cell population committed to the adipocyte lineage and eventually to the hypertrophy of the orbital fat pads (Fig. 6). The changes in the cell lineage commitment also correlates with our finding that OASC populations derived from TAO patients have an increased adipogenic potential and a decreased osteogenic and chondrogenic responses. Compared with previous gene expression profiling studies for WNT pathways, we found a novel dysregulated gene, Wnt1-inducible signaling pathway protein-1 (*WISP1*) in the OASC from TAO patients. The *WISP1* signaling pathway plays a key role in mesenchymal stem cell proliferation as well as adipogenesis.[50] Recent studies suggest that *WISP1* is linked to obesity, inflammation, and insulin resistance.[51] Future studies on *WISP1* dysregulation in the OASC populations derived from TAO patients might provide further insight into the pathophysiology of TAO.

Loss of Early Neural Crest Specifiers in OASC From TAO Patients

Interestingly, compared with adipose tissues in the other parts of the body, orbital fat seems to be the one most affected in TAO patients.[52] Yet, it is still unknown why orbital fat pads show such vulnerability to the systemic immune response in TAO. Other than the tissue components and bony restrictive confines of the orbit, this phenomenon may be partially

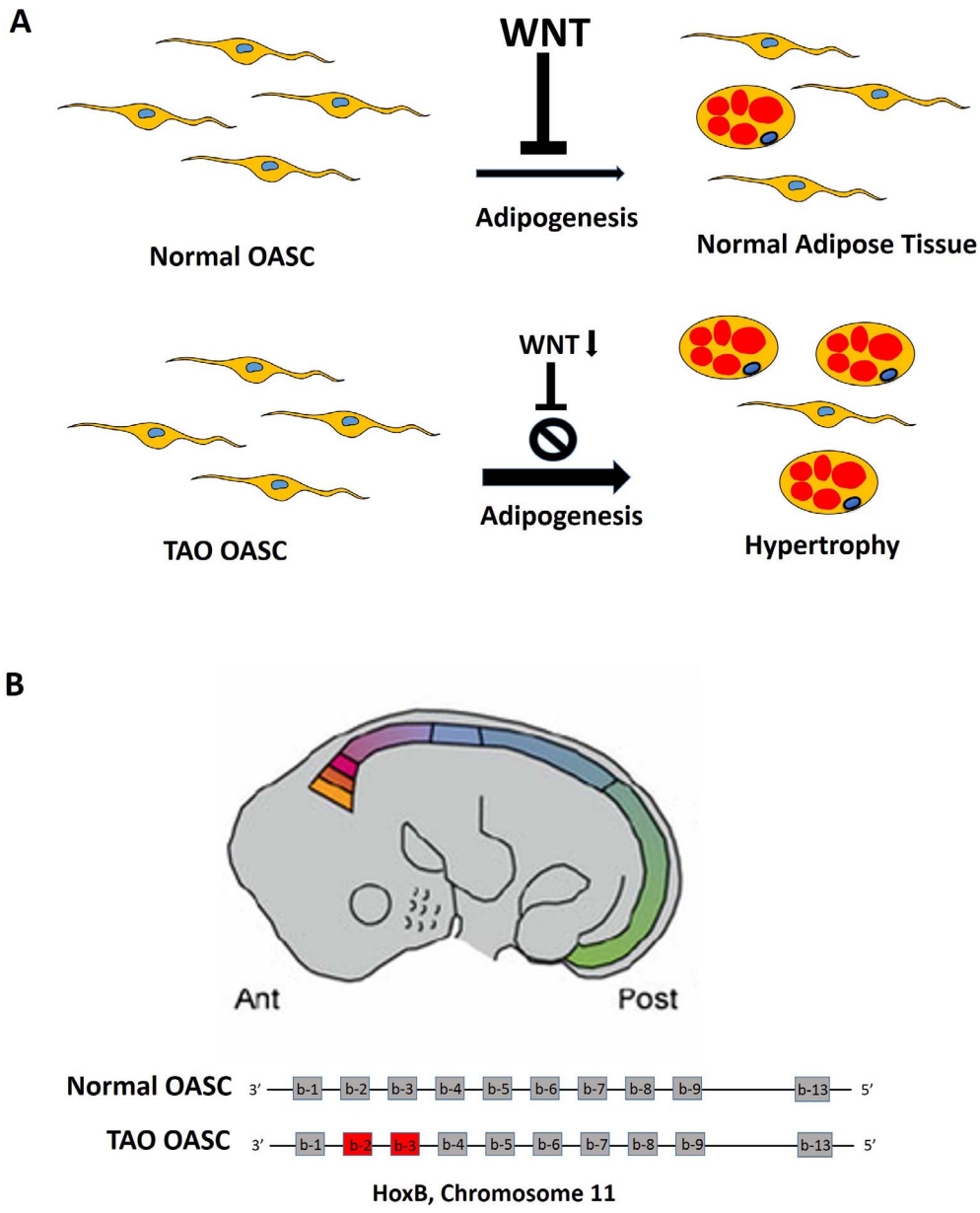

Figure 6. Model for the dysregulation of *HOX* genes and WNT signaling pathways: *HOX* genes: (**A**) canonical WNT signaling regulates the neural crest progenitor cell fate. In the normal OASC, activated WNT/Beta-catenin pathway can suppress commitment to the adipocyte lineage. However, in the OASC from TAO patients, downregulated WNT signaling pathway fail to suppress the adipogenesis pathways in normal OASC, leading to the upregulation of adipogenesis and adipose tissue hypertrophy in the TAO patients. (**B**) The anterior–posterior patterning of *HOXB* gene located on chromosome 11 is illustrated. The diencephalic and mesencephalic neural crest cells give rise to the connective tissues surrounding the eye, including the medial orbital fat pad. During normal development, *HOX* genes expression is normally absent in neural crest cells *HOXB* gene clusters are all gray to show that there is no expression. However, in the TAO patients, the red box indicated that the ectopic expression of *HOXB* gene.

attributed to the unique developmental origin of orbital fat pads. While white adipose tissue was historically considered a homogeneous organ, recent studies indicate that white adipose tissue from each fat depot has its own unique developmental gene expression signature.[53] As with general body patterning in vertebrates, analysis of specific developmental gene expression signatures in the various adipose deposits in the body reveals a strong correlation with site-specific members of the *HOX* gene family.[53,54] In addition, the medial fat pads of the upper eyelid and the lower eyelid fat pads are derived from the migrating cranial neural crest, while the central fat pad in the upper eyelid is derived entirely from mesoderm.[55] The neural crest is a transient population of migrating cells induced at the boundary between the surface ectoderm and neural plate.[56]

Specification of early neural crest progenitor cells begins as early as the gastrula stage: the presumptive neural crest starts to develop at the edges of the neural plate with specification of the neural plate border between neural ectoderm and surface ectoderm.[56,57] As the neural tube forms, progenitors for the neural crest are specified in the dorsal edges of the invaginating neural tube. Later on, cranial neural crest cells undergo an epithelial-to-mesenchymal transformation, delaminate and migrate in a dorsal to ventral manner to produce

craniofacial mesenchyme.[58] These cells give rise to bone, cartilage, nervous structures, and adipose tissue of the face. To specify the neural plate border, signaling molecules like FGFs, WNTs, and bone morphogenetic proteins (BMPs) help establish the presumptive neural crest region.[59] Later on, transcriptional factors such as presumptive neural crest specifier *PAX7*, *ZIC* genes, *MSX2* are activated for neural crest lineage specification.[59] From our data, *WNT* signaling pathways (*WNT16*, *WISP1*), three *ZIC* genes (*ZIC4*, *ZIC2*, *ZIC5*), and one *HOX* gene (*MSX2*) are downregulated in TAO patients. This data could indicate that OASC derived from TAO inherit gene expression signatures with dysregulated neural crest cell developmental pathways, or that OASC reactivate a discordant developmental program in response to the autoimmune process. Regardless, downregulation of these early neural crest specifiers suggests that neural crest lineage specifiers are downregulated in OASC derived from TAO patients.

Ectopic Expression of HOX Genes in OASC From TAO Patients

During the anteroposterior patterning in embryonic development, neural crest cells are induced along the axis, generating nested expression domains of homeobox genes according to their anteroposterior identities.[60,61] Derived from the most anterior segment, cranial neural crest cells give rise to several tissue types surrounding the eye, including bones, cartilage, and connective tissue.[62–64] However, *HOX* gene expression is normally absent in neural crest cells derived from diencephalic, mesencephalic and metencephalic origin.[65,66] *HOXB2* and *HOXB3* are normally expressed up to the boundary between the second and third rhombomere in the hindbrain.[67] Because the expression of *HOX* genes is tightly controlled during development, the ectopic expression of *HOXB2* and *HOXB3* in the OASC derived from TAO patients may be implicated in the pathogenesis and site-specificity of TAO (Fig. 6). Among those developmental genes, *HOXB2* and *HOXB3* are transcriptional factors containing homeobox DNA-binding domains. They are important components of the developmental regulatory network that specifies cellular positions and identities along the anterior–posterior axis.[66,68] Moreover, Iroquois Homeobox 1 (*IRX1*) also belongs to the Iroquois homeobox protein family which is similarly involved in pattern formation during embryo development.[69] Our results show significant dysregulation of *HOX* genes expression in the OASC populations derived from TAO patients. These intrinsic genetic and developmental changes might be implicated in orbital tissue susceptibility in TAO.

Cellular and Developmental Origins of OASC From TAO Patients

Orbital adipose-derived stem cells from normal orbital fat pads and the medial eyelid fat are derived from the migrating cranial neural crest.[55] Orbital adipose-derived stem cells are derived from cranial neural crest origin where *HOX* genes expression is normally absent.[66] Meanwhile, these OASC typically express genes specifying early neural crest identifies, such as *PAX7*, *ZIC* genes, and *MSX2*.[59] However, from our RNA-Seq data, OASC from TAO patients ectopically express *HOX* genes and present a diminished expression of early neural crest specifiers. The following two working models can explain these phenomena: the first model we propose is ectopic expression of *HOX* genes is due to dysregulation in intrinsic epigenetic modifications. In TAO, inflammatory process can activate transcription factors such as nuclear factor kappa-B, FOXP3, IRF, and STAT family proteins. These transcriptional factors can cause epigenetic alteration, including DNA methylation and histone modifications, which are critical in the inflammatory response.[70] These could be attributed to changes of chromatin structure pertaining to the *HOX* gene locus in the OASC from TAO patients. Environmental factors, such as smoking, might affect the epigenetic regulation of *HOX* genes. Another model we propose is that those activated fibroblasts in orbital fat pad from TAO patients are derived from infiltrating fibrocytes, as fibrocytes have been shown to infiltrate the orbit in TAO.[19,71] These CD34+ infiltrating fibrocytes are monocyte-lineages progenitors from the bone marrow that have been found in many aspects of biological processes, such as wound healing, tissue remodeling, and immune functions.[71–73] Because these CD34+ fibrocytes originate from bone marrow but not cranial neural crest, that may explain our data showing that OASC in patients with TAO ectopically express *HOX* genes usually found in the lower segment of the body but do not express early neural crest specifiers. Our results imply that the OASC from TAO patients are derived from hematopoietic lineage instead of neural crest lineages as in the normal orbital adipose tissue. In this case, our model about the involvement of fibrocytes in TAO not only can explain the cellular origin of OASC in TAO but also may shed light on general mechanism of the participation of fibrocytes in other types of autoimmune disease.

Limitations to this study include the small study size and inclusion of patients with both active TAO with compressive optic neuropathy, and patients undergoing orbital rehabilitative surgery. Further studies looking at these pathways stratified by clinical activity score, duration of disease and treatment modality may provide additional information on pathogenic progression. In the current study, subanalysis by these clinical factors did not yield meaningful alterations, likely because of the small study size. While the fact that we did not find a significant difference in gene expression patterns between these two subgroups is likely due to small sample size, it is also possible that activated fibroblasts are the common source that can cause Type 1 and Type 2 TAO by adipogenesis and fibrosis respectively. Our RNA-Seq data revealed mostly intrinsic developmental pathways rather than inflammation genes, and the pathways we found could be general mechanisms that contribute to both subtypes of TAO. Further analysis is necessary to better understand the role of these alterations based on disease subtype and activity.

In conclusion, analysis of the genetic alterations of the OASC, which may have unique multipotency and immunomodulatory roles, can provide a better understanding of the pathophysiology of TAO. Additional studies comparing the local stem cell population with the bone marrow MSC population may provide information regarding the homing of stem cells to areas of disease activity, such as has been well described in other autoimmune diseases.[16,40–42,50] In addition, further analysis of novel dysregulated genes such as *WISP1* may elucidate key targets for therapy.

Acknowledgments

The authors thank Catherine Jeeyun Choi for reading, suggestions, and comments on the manuscript. During the project, several lab members contributed work related to this study, including Michaela Livia Bajenaru, Ravi Doddapaneni, Zenith Acosta Torres, and Galina Dvoriantchikova. The authors also thank Gabriel Gaidosh from the University of Miami Analytical Imaging Core Facility for excellent assistance with confocal microscopy. This work was performed in the Dr. Nasser Al-Rashid Orbital Vision Research Center at the Bascom Palmer Eye Institute.

Supported by grants from the Dr. Nasser Al-Rashid Orbital Research Fund (Miami, FL, USA). Imaging and RGC functional experiments were supported by the National Institutes of Health Center Core Grant P30EY014801 (Bethesda, MD, USA) and Research to Prevent Blindness Unrestricted Grant (New York, NY, USA).

Disclosure: **W. Tao**, None; **J.A. Ayala-Haedo**, None; **M.G. Field**, None; **D. Pelaez**, None; **S.T. Wester**, None

References

1. Stan MN, Bahn RS. Risk factors for development or deterioration of Graves' ophthalmopathy. *Thyroid*. 2010;20:777–783.
2. Bartley GB, Fatourechi V, Kadrmas EF, et al. Clinical features of Graves' ophthalmopathy in an incidence cohort. *Am J Ophthalmol*. 1996;121:284–290.
3. Weetman AP. Graves' disease. *N Engl J Med* 2000;343:1236–1248.
4. Khoo TK, Bahn RS. Pathogenesis of Graves' ophthalmopathy: the role of autoantibodies. *Thyroid*. 2007;17:1013–1018.
5. Forbes G, Gorman CA, Brennan MD, Gehring DG, Ilstrup DM, Earnest F IV. Ophthalmopathy of Graves' disease: computerized volume measurements of the orbital fat and muscle. *AJNR Am J Neuroradiol*. 1986;7:651–656.
6. Wiersinga WM. Autoimmunity in Graves' ophthalmopathy: the result of an unfortunate marriage between TSH receptors and IGF-1 receptors? *J Clin Endocrinol Metab*. 2011;96:2386–2394.
7. Hwang CJ, Afifiyan N, Sand D, et al. Orbital fibroblasts from patients with thyroid-associated ophthalmopathy overexpress CD40: CD154 hyperinduces IL-6, IL-8, and MCP-1. *Invest Ophthalmol Vis Sci*. 2009;50:2262–2268.
8. Pappa A, Lawson JM, Calder V, Fells P, Lightman S. T cells and fibroblasts in affected extraocular muscles in early and late thyroid associated ophthalmopathy. *Br J Ophthalmol*. 2000;84:517–522.
9. Pappa A, Jackson P, Stone J, et al. An ultrastructural and systemic analysis of glycosaminoglycans in thyroid-associated ophthalmopathy. *Eye*. 1998;12(Pt 2):237–244.
10. Hiromatsu Y, Yang D, Bednarczuk T, Miyake I, Nonaka K, Inoue Y. Cytokine profiles in eye muscle tissue and orbital fat tissue from patients with thyroid-associated ophthalmopathy. *J Clin Endocrinol Metab*. 2000;85:1194–1199.
11. Jyonouchi SC, Valyasevi RW, Harteneck DA, Dutton CM, Bahn RS. Interleukin-6 stimulates thyrotropin receptor expression in human orbital preadipocyte fibroblasts from patients with Graves' ophthalmopathy. *Thyroid*. 2001;11:929–934.
12. Hirano T. Interleukin 6 and its receptor: ten years later. *Int Rev Immunol*. 1998;16:249–284.
13. Chatila TA. Interleukin-4 receptor signaling pathways in asthma pathogenesis. *Trends Mol Med*. 2004;10:493–499.
14. Chen MH, Chen MH, Liao SL, Chang TC, Chuang LM. Role of macrophage infiltration in the orbital fat of patients with Graves' ophthalmopathy. *Clin Endocrinol*. 2008;69:332–337.
15. Kumar S, Coenen MJ, Scherer PE, Bahn RS. Evidence for enhanced adipogenesis in the orbits of patients with Graves' ophthalmopathy. *J Clin Endocrinol Metab*. 2004;89:930–935.
16. Kuriyan AE, Woeller CF, O'Loughlin CW, Phipps RP, Feldon SE. Orbital fibroblasts from thyroid eye disease patients differ in proliferative and adipogenic responses depending on disease subtype. *Invest Ophthalmol Vis Sci*. 2013;54:7370–7377.
17. Khong JJ, Wang LY, Smyth GK, et al. Differential gene expression profiling of orbital adipose tissue in thyroid orbitopathy. *Invest Ophthalmol Vis Sci*. 2015;56:6438–6447.
18. Khong JJ, McNab AA, Ebeling PR, Craig JE, Selva D. Pathogenesis of thyroid eye disease: review and update on molecular mechanisms. *Br J Ophthalmol*. 2016;100:142–150.
19. Wang Y, Smith TJ. Current concepts in the molecular pathogenesis of thyroid-associated ophthalmopathy. *Invest Ophthalmol Vis Sci*. 2014;55:1735–1748.
20. Prabhakar BS, Bahn RS, Smith TJ. Current perspective on the pathogenesis of Graves' disease and ophthalmopathy. *Endocr Rev*. 2003;24:802–835.
21. Farid NR, Stone E, Johnson G. Graves' disease and HLA: clinical and epidemiologic associations. *Clin Endocrinol*. 1980;13:535–544.
22. Yanagawa T, Hidaka Y, Guimaraes V, Soliman M, DeGroot LJ. CTLA-4 gene polymorphism associated with Graves' disease in a Caucasian population. *J Clin Endocrinol Metab*. 1995;80:41–45.
23. Brand OJ, Lowe CE, Heward JM, et al. Association of the interleukin-2 receptor alpha (IL-2Ralpha)/CD25 gene region with Graves' disease using a multilocus test and tag SNPs. *Clin Endocrinol*. 2007;66:508–512.
24. Huber AK, Jacobson EM, Jazdzewski K, Concepcion ES, Tomer Y. Interleukin (IL)-23 receptor is a major susceptibility gene for Graves' ophthalmopathy: the IL-23/T-helper 17 axis extends to thyroid autoimmunity. *J Clin Endocrinol Metab*. 2008;93:1077–1081.
25. Liao WL, Chen RH, Lin HJ, et al. Toll-like receptor gene polymorphisms are associated with susceptibility to Graves' ophthalmopathy in Taiwan males. *BMC Med Genet*. 2010;11:154.
26. Douglas RS, Gianoukakis AG, Kamat S, Smith TJ. Aberrant expression of the insulin-like growth factor-1 receptor by T cells from patients with Graves' disease may carry functional consequences for disease pathogenesis. *J Immunol*. 2007;178:3281–3287.
27. Yin X, Latif R, Tomer Y, Davies TF. Thyroid epigenetics: X chromosome inactivation in patients with autoimmune thyroid disease. *Ann N Y Acad Sci*. 2007;1110:193–200.
28. Chitnis S, Monteiro J, Glass D, et al. The role of X-chromosome inactivation in female predisposition to autoimmunity. *Arthritis Res*. 2000;2:399–406.
29. Brix TH, Kyvik KO, Christensen K, Hegedus L. Evidence for a major role of heredity in Graves' disease: a population-based study of two Danish twin cohorts. *J Clin Endocrinol Metab*. 2001;86:930–934.
30. Prummel MF, Wiersinga WM. Smoking and risk of Graves' disease. *JAMA*. 1993;269:479–482.
31. Wakelkamp IM, Gerding MN, van der Meer JW, Prummel MF, Wiersinga WM. Smoking and disease severity are independent determinants of serum adhesion molecule levels in Graves' ophthalmopathy. *Clin Exp Immunol*. 2002;127:316–320.
32. Bufalo NE, Santos RB, Cury AN, et al. Genetic polymorphisms associated with cigarette smoking and the risk of Graves' disease. *Clin Endocrinol*. 2008;68:982–987.
33. Vestergaard P, Rejnmark L, Weeke J, et al. Smoking as a risk factor for Graves' disease, toxic nodular goiter, and autoimmune hypothyroidism. *Thyroid*. 2002;12:69–75.
34. Bartalena L, Martino E, Marcocci C, et al. More on smoking habits and Graves' ophthalmopathy. *J Endocrinol Invest*. 1989;12:733–737.
35. Heyma P, Harrison LC, Robins-Browne R. Thyrotrophin (TSH) binding sites on Yersinia enterocolitica recognized by immunoglobulins from humans with Graves' disease. *Clin Exp Immunol*. 1986;64:249–254.
36. Hargreaves CE, Grasso M, Hampe CS, et al. Yersinia enterocolitica provides the link between thyroid-stimulating

antibodies and their germline counterparts in Graves' disease. *J Immunol*. 2013;190:5373–5381.

37. Ezra DG, Krell J, Rose GE, Bailly M, Stebbing J, Castellano L. Transcriptome-level microarray expression profiling implicates IGF-1 and Wnt signalling dysregulation in the pathogenesis of thyroid-associated orbitopathy. *J Clin Pathol*. 2012;65:608–613.
38. Planck T, Parikh H, Brorson H, et al. Gene expression in Graves' ophthalmopathy and arm lymphedema: similarities and differences. *Thyroid*. 2011;21:663–674.
39. Huber LC, Distler O, Tarner I, Gay RE, Gay S, Pap T. Synovial fibroblasts: key players in rheumatoid arthritis. *Rheumatology*. 2006;45:669–675.
40. Tang Y, Ma X, Zhang H, et al. Gene expression profile reveals abnormalities of multiple signaling pathways in mesenchymal stem cell derived from patients with systemic lupus erythematosus. *Clin Dev Immunol*. 2012;2012:826182.
41. Hou R, Yan H, Niu X, et al. Gene expression profile of dermal mesenchymal stem cells from patients with psoriasis. *J Eur Acad Dermatol Venereol*. 2014;28:1782–1791.
42. Brandau S, Bruderek K, Hestermann K, et al. Orbital fibroblasts from Graves' orbitopathy patients share functional and immunophenotypic properties with mesenchymal stem/stromal cells. *Invest Ophthalmol Vis Sci*. 2015;56:6549–6557.
43. Chen SY, Mahabole M, Horesh E, Wester S, Goldberg JL, Tseng SC. Isolation and characterization of mesenchymal progenitor cells from human orbital adipose tissue. *Invest Ophthalmol Vis Sci*. 2014;55:4842–4852.
44. Romero-Kusabara IL, Filho JV, Scalissi NM, et al. Distinct inflammatory gene expression in extraocular muscle and fat from patients with Graves' orbitopathy. *Eur J Endocrinol*. 2017;176:481–488.
45. Dupin E, Sommer L. Neural crest progenitors and stem cells: from early development to adulthood. *Dev Biol*. 2012;366:83–95.
46. Dorsky RI, Moon RT, Raible DW. Control of neural crest cell fate by the Wnt signalling pathway. *Nature*. 1998;396:370–373.
47. Gaur T, Lengner CJ, Hovhannisyan H, et al. Canonical WNT signaling promotes osteogenesis by directly stimulating Runx2 gene expression. *J Biol Chem*. 2005;280:33132–33140.
48. Ross SE, Hemati N, Longo KA, et al. Inhibition of adipogenesis by Wnt signaling. *Science*. 2000;289:950–953.
49. Kumar S, Leontovich A, Coenen MJ, Bahn RS. Gene expression profiling of orbital adipose tissue from patients with Graves' ophthalmopathy: a potential role for secreted frizzled-related protein-1 in orbital adipogenesis. *J Clin Endocrinol Metab*. 2005;90:4730–4735.
50. Cernea M, Tang W, Guan H, Yang K. Wisp1 mediates Bmp3-stimulated mesenchymal stem cell proliferation. *J Mol Endocrinol*. 2016;56:39–46.
51. Murahovschi V, Pivovarova O, Ilkavets I, et al. WISP1 is a novel adipokine linked to inflammation in obesity. *Diabetes*. 2015;64:856–866.
52. Bahn RS, Heufelder AE. Pathogenesis of Graves' ophthalmopathy. *N Engl J Med*. 1993;329:1468–1475.
53. Yamamoto Y, Gesta S, Lee KY, Tran TT, Saadatirad P, Kahn CR. Adipose depots possess unique developmental gene signatures. *Obesity*. 2010;18:872–878.
54. Karastergiou K, Fried SK, Xie H, et al. Distinct developmental signatures of human abdominal and gluteal subcutaneous adipose tissue depots. *J Clin Endocrinol Metab*. 2013;98:362–371.
55. Korn BS, Kikkawa DO, Hicok KC. Identification and characterization of adult stem cells from human orbital adipose tissue. *Ophthal Plast Reconstr Surg*. 2009;25:27–32.
56. LaBonne C, Bronner-Fraser M. Molecular mechanisms of neural crest formation. *Ann Rev Cell Dev Biol*. 1999;15:81–112.
57. Kalcheim C. Mechanisms of early neural crest development: from cell specification to migration. *Int Rev Cytol*. 2000;200:143–196.
58. Meulemans D, Bronner-Fraser M. Gene-regulatory interactions in neural crest evolution and development. *Dev Cell*. 2004;7:291–299.
59. Huang X, Saint-Jeannet JP. Induction of the neural crest and the opportunities of life on the edge. *Dev Biol*. 2004;275:1–11.
60. Lumsden A, Krumlauf R. Patterning the vertebrate neuraxis. *Science*. 1996;274:1109–1115.
61. Trainor PA, Krumlauf R. Patterning the cranial neural crest: hindbrain segmentation and Hox gene plasticity. *Nat Rev Neurosci*. 2000;1:116–124.
62. Noden DM. Origins and patterning of craniofacial mesenchymal tissues. *J Craniofac Genet Dev Biol Supp*. 1986;2:15–31.
63. Langenberg T, Kahana A, Wszalek JA, Halloran MC. The eye organizes neural crest cell migration. *Dev Dyn*. 2008;237:1645–1652.
64. Creuzet S, Vincent C, Couly G. Neural crest derivatives in ocular and periocular structures. *Int J Dev Biol*. 2005;49:161–171.
65. Hunt P, Gulisano M, Cook M, et al. A distinct Hox code for the branchial region of the vertebrate head. *Nature*. 1991;353:861–864.
66. Creuzet S, Couly G, Vincent C, Le Douarin NM. Negative effect of Hox gene expression on the development of the neural crest-derived facial skeleton. *Development*. 2002;129:4301–4313.
67. Minoux M, Antonarakis GS, Kmita M, Duboule D, Rijli FM. Rostral and caudal pharyngeal arches share a common neural crest ground pattern. *Development*. 2009;136:637–645.
68. Gavalas A, Trainor P, Ariza-McNaughton L, Krumlauf R. Synergy between Hoxa1 and Hoxb1: the relationship between arch patterning and the generation of cranial neural crest. *Development*. 2001;128:3017–3027.
69. Cavodeassi F, Modolell J, Gomez-Skarmeta JL. The Iroquois family of genes: from body building to neural patterning. *Development*. 2001;128:2847–2855.
70. Medzhitov R, Horng T. Transcriptional control of the inflammatory response. *Nat Rev Immunol*. 2009;9:692–703.
71. Smith TJ. TSH-receptor-expressing fibrocytes and thyroid-associated ophthalmopathy. *Nat Revs Endocrinol*. 2015;11:171–181.
72. Fernando R, Atkins SJ, Smith TJ. Intersection of chemokine and TSH receptor pathways in human fibrocytes: emergence of CXCL-12/CXCR4 cross talk potentially relevant to thyroid-associated ophthalmopathy. *Endocrinology*. 2016;157:3779–3787.
73. Gillespie EF, Papageorgiou KI, Fernando R, et al. Increased expression of TSH receptor by fibrocytes in thyroid-associated ophthalmopathy leads to chemokine production. *J Clin Endocrinol Metab*. 2012;97:E740–E746.

Investigative Ophthalmology & Visual Science